Seismic modeling and inversion for reflections from fractures

Xiaoqin (Jean) Cui, Laurence R. Lines and Edward S. Krebes

ABSTRACT

We have studied a theory of linear slip nonwelded contact interfaces (Schoenberg, 1980) and extended the theory to simulate the subsurface fracture features by developing a 2D/3D numerical forward modeling method and a method of analysis of the PP and PS seismogram characteristics regarding the responses of the fractures (Cui, Lines and Krebes, 2012). In this paper we present a new AVO inversion equation that depends upon the theory of the linear slip nonwelded contact interfaces. We use the assumption that the two half spaces are in imperfect contact due to the presence of fractures, meaning that only the stresses produced by the wave are continuous across a fracture, and that the displacements are discontinuous across the fracture. The new equation can be inverted not only to estimate the subsurface elastic parameters contrasts, but also to estimate eight parameters related to the fractured media. This paper analyses fracture models and compares the results of numerical forward modeling between media with interfaces in perfect welded contact (no fractures) and with interfaces in imperfect linear slip nonwelded contact (with fractures). Inversion results of three models are also compared.

INTRODUCTION

The upper crust of the earth is considerably layered with complex geometry interfaces between layers with different elastic parameters as well as a single layer medium with a unique elastic parameter. The two half spaces in the limit of the interface either are in perfectly welded contact or are in imperfect non-welded contact. In 1980, Schoenberg in his pioneering work produced a theory of the linear slip non-welded contact interface, where the particle displacements are discontinuous across interface and the stresses are continuous across it. Additionally, the particle displacements are linearly proportional to the stresses in which the linear coefficients are named as specific tangential compliance S_T and normal compliance S_N, that are important parameters describing a fracture system. Also, as shown by Schoenberg and Douma (1988), S_T and S_N incorporate the displacement discontinuity of the penny-shaped crack model (Hudson, 1980), as well as Thomson's anisotropic parameters ε, δ and γ (Thomson, 1985). The PP and PS reflection and transmission coefficients in the anisotropic VTI and HTI media with the theory of the linear slip nonwelded contact interface have been presented in 2011 (Cui and Lines, 2011). Pyrak-Nolte (1990) has confirmed the model to be a non-welded contact interface theory by performing laboratory measurements. Schoenberg and Muir (1989) presented the group theory formula based on the effective medium theory (Backus, 1962) to conveniently calculate the elastic moduli for the fractured and unfractured media. Nichols et al. (1989) and Hood (1991) show the solutions of the elastic moduli for a vertical fracture as a linear slip non-welded contact interface vertically embedded in the background medium. Schoenberg and Sayers (1995) expanded Hooke's Law with the linear slip theory to find a relationship of the fracture compliances S_T, S_N with Young's modulus, Poisson's ratio of the rock parameters. Coates and Schoenberg (1995) applied the linear slip approach with equivalent medium theory to generate seismograms by employing the finite difference method with a staggered grid. Slawinski and Krebes

(2002) simulated seismograms of SH and P-SV wave propagation in the linear slip non-welded contact interface by using 2D generalized homogeneous finite difference schemes. The fractured parameters S_T and S_N can be estimated through an azimuthal simultaneous elastic inversion (Downton and Roure, 2010). In 2012, David Gray developed a method to estimate crucial stress and geomechanical properties in anisotropic media by employing the fractured parameters S_T and S_N. A complex 3D fractal network wormhole model for the cold heavy oil production with sand (CHOPS) has been simulated that assumed three different directions of the fracture and this model is consistent with the phenomena of wormholes (Cui, Lines and Krebes, 2012).

The AVO method depending on the Zoeppritz equation is a very powerful tool to analyze the change in the offset that is dependent on the reflectivity along the interface. Studying of the seismic forward modeling not only can analyze the recorded wave characteristics, but also can invert the seismic reflection data to produce elastic parameters of the target, such as velocity reflectivity, impedance reflectivity. Therefore, approximations to the Zoeppritz equation with the relatively higher accuracy are desirable in the practice of amplitude inversion. Aki and Richards (1980) published three parameters AVO inversion equations by the linear approximation of the Zoeppritz equation. Shuey (1985) further modified the Aki and Richards's equation by using Poisson's ratio. Smith and Gidlow (1987) rearranged the Aki and Richards's equation and applied an empirical relationship (Gardner et al, 1974) to the simplified AVO equation as the two parameters impedance reflectivity. The exact solution of the reflection coefficients with the theory of the linear slip nonwelded contact interface has been discussed in 2002 (Chaisri). In this paper, we present amplitude AVO approximation expressions that have same terms, the offset dependent and approximated, as Aki and Richards's AVO equation.

THEORY: FORWARD MODELING

A conventional wave that propagates at a perfect welded contact interface, the boundary conditions are continuous for both displacements and stresses. Whereas the boundary conditions of the linear slip nonwelded contact interface approach (Schoenberg, 1980), where only the stresses are continuous across the interface, but the displacements are not. All displacements are the linear function of the stresses i.e.

$$U^{x+} - U^{x-} = S_T \sigma^{zx+(-)} \quad (1a)$$

$$U^{z+} - U^{z-} = S_N \sigma^{zz+(-)} \quad (1b)$$

$$\sigma^{zx+(-)} = \sigma^{zx-(+)} \quad (1c)$$

$$\sigma^{zz+(-)} = \sigma^{zz-(+)} \quad (1d)$$

Where

$$\sigma^{zx} = \mu\left(\frac{\partial U^z}{\partial x} + \frac{\partial U^x}{\partial z}\right) \quad (2a)$$

$$\sigma^{zz} = \lambda \frac{\partial U^x}{\partial x} + (\lambda + 2\mu) \frac{\partial U^z}{\partial z} \quad (2b)$$

U and Ϭ express the displacement and stress, respectively. x, z are two components along the horizontal and vertical directions. μ and λ are lambda and mu as the rock properties. S_T and S_N are two complex frequency dependent interface compliance (Schoenberg, 1980). Sign + and – denote the upper and the lower media of the interface, respectively. Substituting equations 2 to for equation (1), where the difference in displacement of x and z components at the interface

$$U^{x+} - U^{x-} = S_T \mu (\partial_x U^z + \partial_z U^x) \quad (3a)$$

$$U^{z+} - U^{z-} = S_N (\lambda \partial_x U^x + (\lambda + 2\mu) \partial_z U^z) \quad (3b)$$

Using the generalized homogeneous FD algorithm (Korn and Stockl, 1982) to form a linear slip non-welded contact fracture at $z_{n+1/2} = (n + 1/2)\Delta z$ (Slawinski and Krebes, 2002),

$$\begin{aligned} \Delta U^x_{m,n+1/2} &= \frac{1}{2}\left(U^x_{m,n+1} + \tilde{U}^x_{m,n}\right) - \frac{1}{2}\left(\tilde{U}^x_{m,n+1} + U^x_{m,n}\right) \\ &= z_T \mu_{m,n+1}\left(\frac{U^z_{m+1,n+1} - U^z_{m-1,n+1}}{2\Delta x} + \frac{U^x_{m,n+1} - \tilde{U}^x_{m,n}}{\Delta z}\right) \\ &= z_T \mu_{m,n+1}\left(\frac{\partial U_z}{\partial x} + \frac{\partial U_x}{\partial z}\right) \end{aligned} \quad (4a)$$

$$\sigma^{xz}_{m,n+1} = z_T \mu_{m,n+1}\left(\frac{U^z_{m+1,n+1} - U^z_{m-1,n+1}}{2\Delta x} + \frac{U^x_{m,n+1} - \tilde{U}^x_{m,n}}{\Delta z}\right) \quad (4b)$$

Where, m and n denote real grid points along the x and y axis, respectively. $\mu_{m,n} = \mu_{m,n+1} = \mu$, $\lambda_{m,n} = \lambda_{m,n+1} = \lambda$ are the isotropic medium parameters. $\tilde{U}^x_{m,n}$ and $\tilde{U}^x_{m,n+1}$ are displacements as a fictitious point that have same location as real grid $U^x_{m,n}$ and $U^x_{m,n+1}$. The compliances S_T and S_N are nonzero constants for all boundaries that exist between the grid rectangles. So the fictitious points of x-component (Equation 4) for z-normal grid boundary (a horizontal fracture) $\tilde{U}^x_{m,n}$ and $\tilde{U}^x_{m,n+1}$ can be solved since there are two equations with two unknown fictitious points. Let $\Delta x = \Delta z = h$, and $\delta = \frac{z_T \mu}{h}$, and $Ø = \frac{z_N(\lambda+2\mu)}{h}$, then the fictitious points $\tilde{U}^x_{m,n}$ and $\tilde{U}^x_{m,n+1}$ are replaced by real grid points $U^x_{m,n}$ and $U^x_{m,n+1}$for the z-normal boundary or horizontal fracture. To be similar to $\tilde{U}^z_{m,n}$

and $\widetilde{U}^{z}_{m+1,n}$. Thus the FD scheme of the P-SV propagation in the homogeneous medium with a linear slip non-welded contact interface should be

$$\mathbf{U}^{t+1}_{m,n} = -\mathbf{U}^{t-1}_{m,n} + 2\mathbf{U}^{t}_{m,n} + \frac{1}{\rho}\left(\frac{\Delta t}{h}\right)^2\left(\mathbf{F}\widehat{\mathbf{N}}\mathbf{F}(\mathbf{U}^{t}_{m+1,n} - 2\mathbf{U}^{t}_{m,n} + \mathbf{U}^{t}_{m-1,n})\right.$$
$$+\widehat{\mathbf{N}}(\mathbf{U}^{t}_{m,n+1} - 2\mathbf{U}^{t}_{m,n} + \mathbf{U}^{t}_{m,n-1})$$
$$\left.+\frac{1}{4}(\mathbf{F}\widehat{\mathbf{G}}\mathbf{F} + \widehat{\mathbf{G}})(\mathbf{U}^{t}_{m+1,n+1} - \mathbf{U}^{t}_{m+1,n-1} - \mathbf{U}^{t}_{m-1,n+1} + \mathbf{U}^{t}_{m-1,n-1})\right) \quad (5)$$

Where $\mathbf{U} = \begin{bmatrix} U^x \\ U^z \end{bmatrix}$, $\mathbf{F} = \begin{bmatrix} 0 & 1 \\ 1 & 0 \end{bmatrix}$, $\widehat{\mathbf{N}} = \begin{bmatrix} \frac{\mu}{1+\delta} & 0 \\ 0 & \frac{\lambda+2\mu}{1+\emptyset} \end{bmatrix}$, $\widehat{\mathbf{G}} = \begin{bmatrix} 0 & \frac{\mu}{1+\delta} \\ \frac{\lambda}{1+\emptyset} & 0 \end{bmatrix}$.

Adding fictitious grid points in the FD scheme takes more physical insights into account to the fracture forward modeling because the medium and boundary conditions (BCs) are imposed explicitly. The equation of motion governs the displacements off the discontinuity fracture but the non-welded contact boundary conditions are applied at the discontinuity fracture.

THEORY: AVO INVERSION

A compressional wave source going down the incidence and generate the reflected and transmitted four waves at the interface z. Figure 1 shows the incident a plane wave $p\grave{}_1$, the reflected waves $p\grave{}_1p\acute{}_1$, $p\grave{}_1s\acute{}_1$ and the transmitted waves $p\grave{}_1p\grave{}_2$, $p\grave{}_1s\grave{}_2$. The media parameters are $\alpha_1, \beta_1, \rho_1$ and $\alpha_2, \beta_2, \rho_2$ for the upper and lower medium respectively. i_1 is incident angle, j_1 is $p\grave{}_1s\acute{}_1$ reflection angle. The $p\grave{}_1p\acute{}_1$ and $p\grave{}_1s\acute{}_1$ amplitude reflectivity are also represented as a function of the elastic contrasts at an interface and be used to derive the linear approximation for conventional amplitude variation with offset (AVO) analysis, which can inverse for two or three elastic parameters.

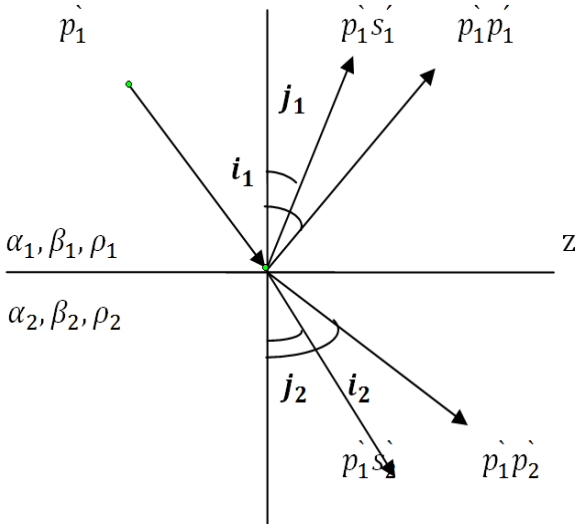

Fig 1 Reflected and transmitted rays for an incident $p_1^{`}$-wave on an interface Z between two elastic isotropic media $\alpha_1, \beta_1, \rho_1$ and $\alpha_2, \beta_2, \rho_2$.

Following the descriptions in Krebes's course note book Geophysics 551, we use the harmonic wave to represent an incident and a plane wave $p_1^{`} = A\exp(iw(\mathbf{s}.\mathbf{x} - t)\,\mathbf{d})$. Where A is the amplitude and assumed to be a unit. $\mathbf{s}.\mathbf{x} = \mathrm{s_x x} + \mathrm{s_y y} + \mathrm{s_z z}$ describes a harmonic plane wave in the travel direction and **d** is for the wave polarization. Applying the linear slip nonwelded contact interface boundary condition (1) at interface z, the Zoeppritz equation is the result in the relationship of P-SV waves with the fracture parameters S_T and S_N (Schoenberg, 1980. Chaisri, 2002)

$$\begin{bmatrix} \alpha_1 \mathrm{P} \\ \cos i_1 \\ x_1 \cos i_1 \\ \alpha_1 r_1 \end{bmatrix} =$$

$$\begin{bmatrix} -\alpha_1 \mathrm{P} & -\cos j_1 & \alpha_2 \mathrm{P} - I\omega S_X x_2 \cos i_2 & \cos j_2 - I\omega S_X \beta_2 r_2 \\ \cos i_1 & -\beta_1 \mathrm{P} & \cos i_2 - I\omega S_N \alpha_2 \gamma_2 & -\beta_2 \mathrm{P} - I\omega S_N x_2 \cos j_2 \\ x_1 \cos i_1 & \beta_1 r_1 & x_2 \cos i_2 & \beta_2 r_2 \\ -\alpha_1 r_1 & x_1 \cos j_1 & \alpha_2 r_2 & -x_2 \cos j_2 \end{bmatrix} \begin{bmatrix} \mathrm{P_1^{`}P_1^{'}} \\ \mathrm{P_1^{`}S_1^{'}} \\ \mathrm{P_1^{`}P_2^{`}} \\ \mathrm{P_1^{`}S_2^{`}} \end{bmatrix} \qquad (6)$$

$I\omega S_{X(N)}$ always appear in combination meaning the S_X and S_N frequency dependent (Chaisri, 2002). Where $I = \sqrt{-1}$. $P = \frac{\sin i_n}{\alpha_n} = \frac{\sin j_n}{\beta_n}$ is ray parameter. $x_n = 2\rho_n \beta_n^2$, $r_n = \rho_n(1 - 2\beta_n^2 P^2)$, and n=1 or 2 denote upper and lower media. The left matrix of these equations is the incident wave and the right matrix is the scattered wave. Simplified above matrix equation,

$$\mathrm{M}[\mathrm{P_1^{`}P_1^{'}} \quad \mathrm{P_1^{`}S_1^{'}} \quad \mathrm{P_1^{`}P_2^{`}} \quad \mathrm{P_1^{`}S_2^{`}}]^{\mathrm{T}} = \mathrm{N},$$

or

$$\mathrm{MX{=}N}$$

According to Cramer's rule, $\mathrm{X_k} = \frac{\det(\mathrm{M_k})}{\det(\mathrm{M})}$. $\mathrm{M_k}$ is the matrix M with column k replaced by the column vector N. Thus,

$$\mathrm{P_1^{`}P_1^{'}} = \frac{\det(\mathrm{M_{N-pp}})}{\det(\mathrm{M})} = \frac{\begin{bmatrix} \mathrm{N_{11}} & \mathrm{m_{12}} & \mathrm{m_{13}} & \mathrm{m_{14}} \\ \mathrm{N_{21}} & \mathrm{m_{22}} & \mathrm{m_{23}} & \mathrm{m_{24}} \\ \mathrm{N_{31}} & \mathrm{m_{32}} & \mathrm{m_{33}} & \mathrm{m_{34}} \\ \mathrm{N_{41}} & \mathrm{m_{42}} & \mathrm{m_{43}} & \mathrm{m_{44}} \end{bmatrix}}{\det(\mathrm{M})} \qquad (7a)$$

$$\mathrm{P_1^{`}S_1^{'}} = \frac{\det(\mathrm{M_{N-ps}})}{\det(\mathrm{M})} = \frac{\begin{bmatrix} \mathrm{m_{11}} & \mathrm{N_{12}} & \mathrm{m_{13}} & \mathrm{m_{14}} \\ \mathrm{m_{21}} & \mathrm{N_{22}} & \mathrm{m_{23}} & \mathrm{m_{24}} \\ \mathrm{m_{31}} & \mathrm{N_{32}} & \mathrm{m_{33}} & \mathrm{m_{34}} \\ \mathrm{m_{41}} & \mathrm{N_{42}} & \mathrm{m_{43}} & \mathrm{m_{44}} \end{bmatrix}}{\det(\mathrm{M})} \qquad (7b)$$

Straight forward to solve linear algebraic Equation (7a) for PP wave, the exact reflectivity solution of PP wave propagation at the fracture

$$\mathrm{P_1`P_1'} = \mathrm{R}_w + i\omega S_X \mathrm{R}^x_{non\_w} + i\omega S_N \mathrm{R}^N_{non\_w} \quad (8)$$

Equation (8) contains conventional perfect welded contact amplitude reflectivity R_w and unconventional imperfect nonwelded contact amplitude reflectivity $\mathrm{R}^{\mathrm{x}}_{non\_w}$ and $\mathrm{R}^{\mathrm{N}}_{non\_w}$ with the fracture parameters combination S_T and S_N, respectively. X , N upper subscript indicates the tangential and normal components. In the amplitude reflectivity of the perfect welded contact part R_w, it assumed that all incident and transmission angles are real and less than 90^0(Aki and Richards, 1980), and it followed

$$\Delta i = i_2 - i_1 = \tan i \frac{\Delta\alpha}{\alpha}$$

$$\Delta j = j_2 - j_1 = \tan j \frac{\Delta\beta}{\beta}$$

$\alpha = \frac{\alpha_2+\alpha_1}{2}$, $\beta = \frac{\beta_2+\beta_1}{2}$, $\rho = \frac{\rho_2+\rho_1}{2}$, $\Delta\alpha = \alpha_2 - \alpha_1$, $\Delta\beta = \beta_2 - \beta_1$, $\Delta\rho = \rho_2 - \rho_1$,

Then,

$$\mathrm{R}_w(t) \approx \frac{1}{2}\left(1 - 4\left(\frac{\beta}{\alpha}\right)^2 \sin^2 i\right)\frac{\Delta\rho}{\rho} + \frac{1}{2\cos^2 i}\frac{\Delta\alpha}{\alpha} - 4\left(\frac{\beta}{\alpha}\right)^2 \sin^2 i \frac{\Delta\beta}{\beta}$$
$$= \mathrm{A}(i)r_\alpha + \mathrm{B}(i)r_\beta + \mathrm{C}(i)r_\rho = \widetilde{\mathrm{R}_w}(t)$$

Where r_α, r_β and r_ρ are compressional, shear velocity and density reflectivity. A, B and C is function of incident angle and depends on the background model or geometry.

As the imperfect nonwelded contact interface parts, it deduced as same approximation as the perfect part R_w to the ray parameter p.

$$\mathrm{R}^{\mathrm{x}}_{non\_w}(t) \approx \mathrm{X}(i) + \mathrm{A}^{\mathrm{x}}(i)r_\alpha + \mathrm{B}^{\mathrm{x}}(i)r_\beta + \mathrm{C}^{\mathrm{x}}(i)r_\rho = \widetilde{\mathrm{R}^{\mathrm{x}}_{non\_w}}(t)$$
$$\mathrm{R}^{\mathrm{N}}_{non\_w}(t) \approx \mathrm{N}(i) + \mathrm{A}^{\mathrm{N}}(i)r_\alpha + \mathrm{B}^{\mathrm{N}}(i)r_\beta + \mathrm{C}^{\mathrm{N}}(i)r_\rho = \widetilde{\mathrm{R}^{\mathrm{N}}_{non\_w}}(t)$$

$\widetilde{\mathrm{R}^{\mathrm{x}}_{non\_w}}$ and $\widetilde{\mathrm{R}^{\mathrm{N}}_{non\_w}}$ are arranged terms as r_α, r_β and r_ρ as following normal perfect welded contact part approximation $\widetilde{\mathrm{R}_w}$, thus the equation (8) can be redefined

$$\mathrm{P_1`P_1'} \approx \widetilde{\mathrm{R}_w} + i\omega S_X \widetilde{\mathrm{R}^{\mathrm{x}}_{non_w}} + i\omega S_N \widetilde{\mathrm{R}^{\mathrm{x}}_{non_w}} =$$

$$(i\omega S_X \mathrm{X}(i) + i\omega S_N \mathrm{N}(i)) +$$
$$(\mathrm{A}(i) + i\omega S_X \mathrm{A}^{\mathrm{x}}(i) + i\omega S_N \mathrm{A}^{\mathrm{N}}(i))r_\alpha +$$
$$(\mathrm{B}(i) + i\omega S_X \mathrm{B}^{\mathrm{x}}(i) + i\omega S_N \mathrm{B}^{\mathrm{N}}(i))r_\beta +$$
$$(\mathrm{C}(i) + i\omega S_X \mathrm{C}^{\mathrm{x}}(i) + i\omega S_N \mathrm{C}^{\mathrm{N}}(i))r_\rho \quad (9)$$

The fractured interface amplitude reflectivity $\mathrm{P_1`P_1'}$ depends on incident angle and plus the fluctuations of the fracture. Figure 2 shows the PP wave reflection coefficient curves that are the exact solution in Equation 6 and the approximation solution in Equation 9 of the

linear slip nonwelded contact interface with a certain frequency. This proved that the AVO approximation Equation 9 of the nonwelded contact linear slip interface reaches accuracy in conventional incident angle range.

Let $r_\alpha = r_\beta = r_\rho = 0$,

$$\mathrm{P_1\grave{P}_1\acute{}} \approx i\omega S_X \mathrm{X} + i\omega S_N \mathrm{N} \tag{10}$$

Equation 10 clearly expresses that the fractures can be detected even though the fractures are embedded in a single medium with non impedance contrast. The fracture features cause a phase change because of a complex number that carries on the amplitude and phase properties of a signal.

The geologic factors and their corresponding elastic parameters, such as velocities reflectivity, density reflectivity at the interface, are the ultimate objective of geoscience. It is not hard to do the amplitude inversion because the amplitude reflectivity Equation 9 approximated to the elastic parameters reflectivity format as the compression velocity reflectivity, the shear velocity reflectivity and the density reflectivity. Equation 9 rewrites

$$Gm = d \tag{11}$$

G as a linear operator depending on the geometry. m is the unknown parameter, for example, r_α, r_β and r_ρ. d is the received seismic data. Least squares method was employed to solve Equation 11

$$G^T G m = G^T d$$

$$m = [G^T G]^{-1} G^T d$$

$$\begin{bmatrix} r_\alpha \\ r_\beta \\ r_\rho \end{bmatrix} = [G^T G + \lambda I]^{-1} G^T d \tag{12}$$

The addition of a matrix λI tends to stabilize the calculation of $[G^T G]^{-1}$ (Lines and Treitel, 1984). The Equation 12 can solve eight unknown elastic parameters and the description media will ignore the density changing, such as fracture parameters S_T, S_N, common velocities reflectivity, r_α, r_β and four fractured velocities reflectivity (fracture compliance multiplying velocities reflectivity).

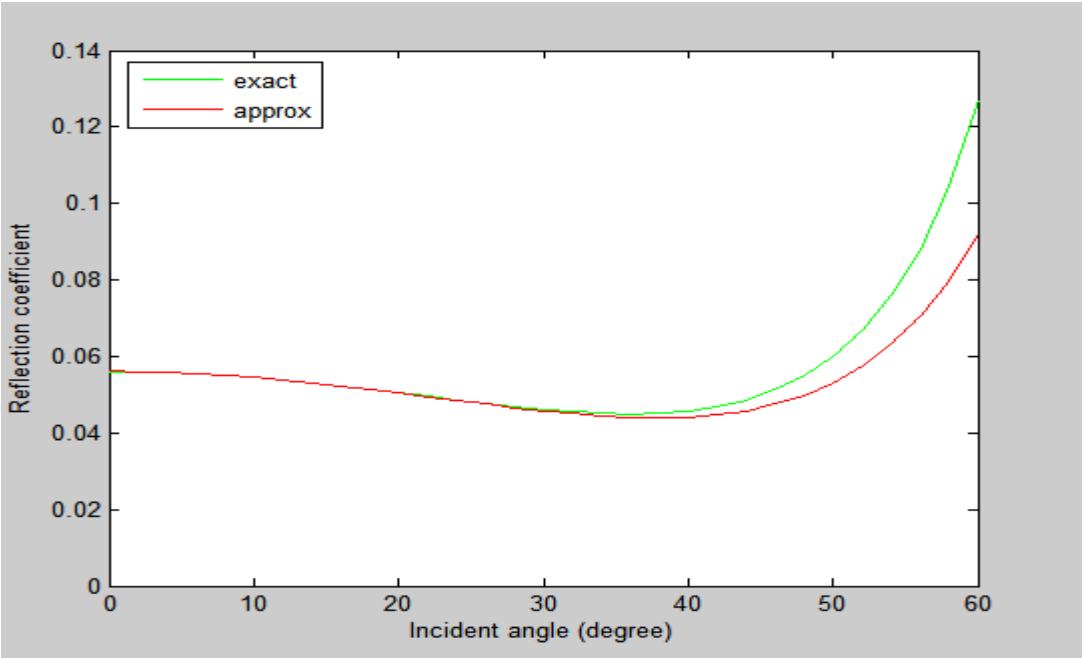

FIG. 2. PP reflection coefficients for the linear slip nonwelded contact interface. Shown are the exact solution (green line, equation (6)), the approximation solution (red line) based on equation (9). The model parameters are Vp1=3100m/s, Vs1=1500m/s, Vp2=2900m/s, Vs2=1300m/s, $S_T = 0.127\text{x}10^{-8}$ m/Pa, $S_N = 0.269\text{x}10^{-9}$m/Pa

APPLICATIONS

We have implemented the Matlab code to present numerical results for both modeling and inversion. The homogeneous isotropic medium parameters have shown in Figure 3. The fracture parameters $S_T = 0.127\text{x}10^{-8}$ m/Pa and $S_N = 0.269\text{x}10^{-9}$m/Pa. The finite difference scheme depends on the discrete grid variable (Lines, Slawinski and Bording, 1999). In order to avoid a problem of the FDs edge effects, it is helpful to extend spatial grids until the effective primary wave is reflected from the fracture without the interfering coming from the four edge reflections. Thus the geometry has 400x400 spatial grids, its steps are $\Delta x=\Delta z=h=5.0$ m and the time step is 0.0001ms. The source is located at the 175x200 of the model. The receiver arrays are arranged horizontally above the source at a distance of 10 grids. The Ricker wavelet was introduced as a source wavelet that is generated from an analog expression and using the CREWES software. Ricker $(t)=(1-2\Pi^2 f^2 t^2)\exp(-\Pi^2 f^2 t^2)$. (See CREWES software: wavenorm.m). We set up three models: the model one works on only an impedance contrast interface; the model two is for a combination of the impedance contrast and a horizontal fracture at the same depth; the model three merely works for a fracture embedded in a single homogeneous medium.

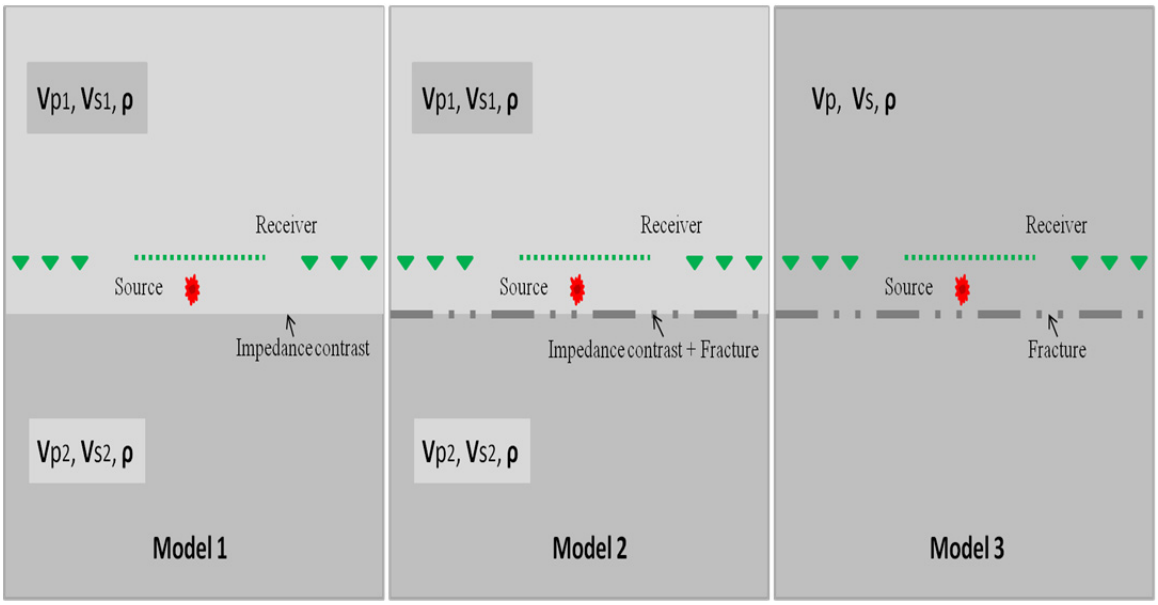

FIG. 3. Models. Model 1 is a case of the normal perfect welded contact impedance contract. Model 2 is a combination case of the perfect welded contact and imperfect nonwelded contact interface. Model 3 is a case of a fracture embedding in single homogenous medium. .

As we know, the seismogram recorded the seismic wave as being sensitive to the impedance contrast at the interface, but it is convolution of the wavelet and the interface reflectivity. To address the wavelet factors of the seismic data must properly be conditioned or processed to meet the assumptions inherent in the AVO model. A practical implementation issue is the undoing of the convolution to remove the wavelet effects from the seismic data and get back to the true reflectivity series so that ideally the seismic wavelet should have a uniform amplitude spectrum and a consistent phase in the seismic records.

For a better understanding of the fracture's properties, it is useful to investigate numerically PP and PS amplitude variation in the synthetic seismograms from three models. Figure 4 shows raw shot records, deconvolution processed shot records and their spectrum analysis in three columns (for three models) and three rows (showing raw, decon shots and their amplitude spectrum). The shot records demonstrate that the amplitude is a variation with the incident angle and PP has stronger amplitude than PS. The shot record of the model 3 (m3) is clear that the fracture feature is reflection generator to result in seismic reflectivity. The reason is due to the displacement discontinuity across the fracture, even though model 3 has not the impedance contrast to create seismic reflections. The amplitude spectrum illustrate that deconvolution enhance the frequency width and get amplitude spectrum close white, while the rest abnormal amplitude are reflecting the subsurface structure. For example, the deconvoluted amplitude spectrums of the model 3 (green color) showing notches are explicit that the subsurface fracture cause the wave amplitude frequency dependent. We also study that the fractured interface model 2 is a linear combination in a fracture (the model 3) and an impedance contrast interface (the model 1). The waves from three models with a certain frequency are exhibited in the Figure 5: The blue line is showing a wave of the model 1 as a pure impedance contrast interface. The solid red line is displaying a wave of the

model 2 as the fractured impedance contrast interface. The green line is a presentation of a wave of the model 3 for a fracture. The summation of model 1 and model 3 result in the red dash line that is almost equal to the red solid line being model 2. Figure 6 shows the muted CDP gathers that have PP reflections and 120 fold for each model.

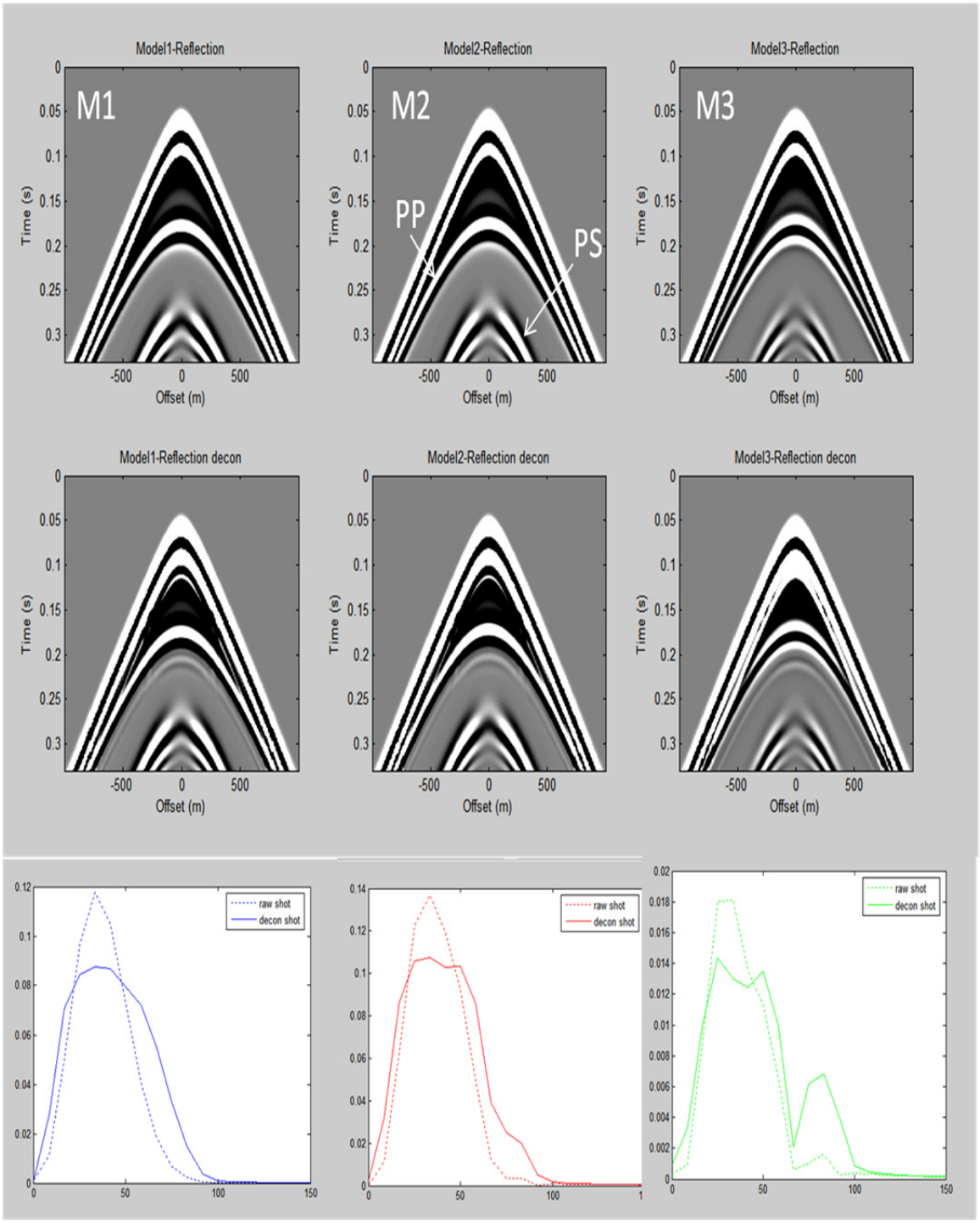

Fig. 4. Three models raw shot records on the first row. Three processed deconvolution shot data on the second row. The third row shows spectrum analysis for three model shot records.

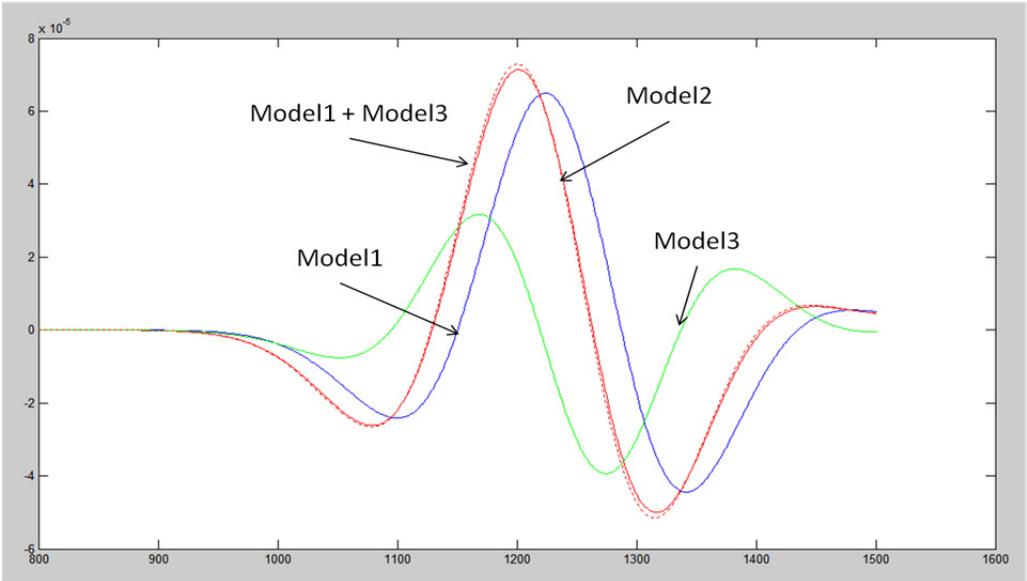

FIG. 5. Model1 + Model3 =Model2. The blue line is showing a wave of the model1 as an impedance contrast interface. The solid red line is displaying a wave of the model 2 as fractured impedance contrast interface. The green line is presentation of a wave of the model 3 for merely fracture. The summation of model 1 and model3 result in the red dash line that is almost equal to red solid line being model 2.

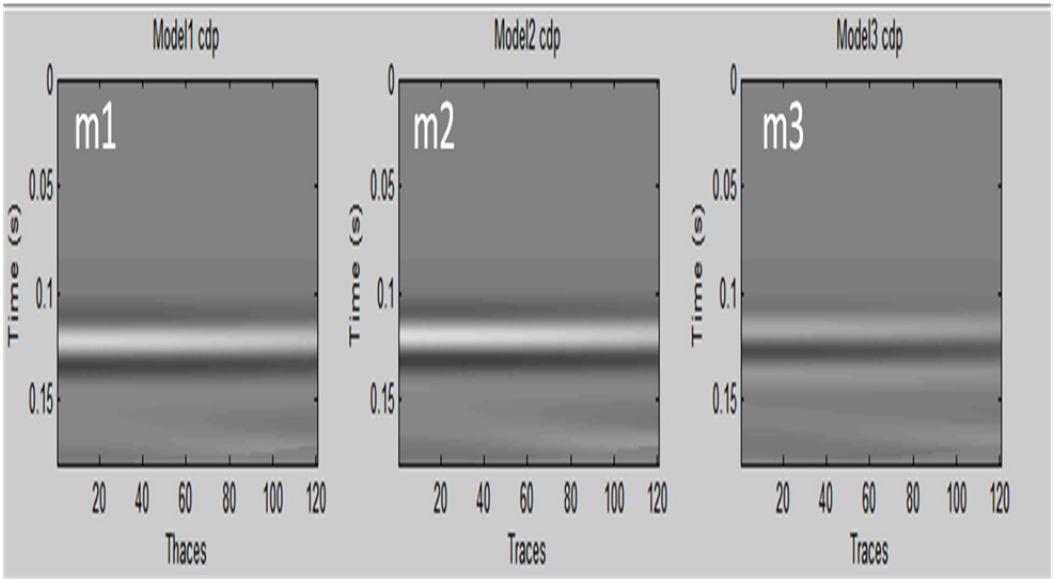

FIG. 6. CDP gathers are for three models.

Three synthetic seismograms have been decomposed individually into a single frequency in order to satisfy a demanding of the AVO inversion Equation 10, and the summation of all components of the AVO inversion results as the elastic parameters description for each model

Figure 7 is the inversion result of the model 1. Both the P wave reflectivity and the shear wave reflectivity indicate that an impedance contrast interface media parameters has been inverted at 137 ms in time. Model 2, is the fractured impedance contrast interface, and inversion results have been presented in the Figure 8. a2 and b2 represent the elastic velocities reflectivity at the fractured impedance contrast interface. c2 and d2 are fractured parameters that imply a fracture exists and its parameter S_T and S_N can be solved by surface record seismic data. e2 and f2 are the inversed solution of the fracture compliances multiplying the P wave velocity reflectivity, as well as g2 and h2 are the fracture compliances multiplying the shear wave velocity reflectivity. Those eight inversion results provide extra information to indicate the subsurface fractures. We discussed above that the linear slip nonwelded contact interface is a reflector to generate the reflection being recorded at the surface. The records has been inversed and shown in the Figure 9. a3 is for tangential compliance S_T by inversion of the record of the model 3, as well as b3 is the inversion result for the normal compliance S_N.

CONCLUSIONS

The fracture as a linear slip nonwelded contact interface has been studied and simulated. This work helps us not only to learn the subsurface fracture characterizations, but also to research new AVO inversion methods under the linear slip nonwelded contact interface theory. The new AVO approximation equation is accurate in the conventional incident angle by the comparison exact solution with its approximation solution. The new AVO method inversion can solve more than six elastic parameters except the conventional P and shear wave velocity reflectivity. Those inversion results obviously describe the medium elastic and fractured properties. Thus this research can help us to indicate the existing fracture and contribute to the analysis of the reservoir permeability characterization.

ACKNOWLEDGMENTS

We would like to thank the sponsors of CREWES and CHORUS. Thanks to Peng Cheng for the Matlab coding and discussion of the signal theory. Thanks to Peter Manning for FD Staggered grid coding. Thanks to Joan Embleton for the English corrections.

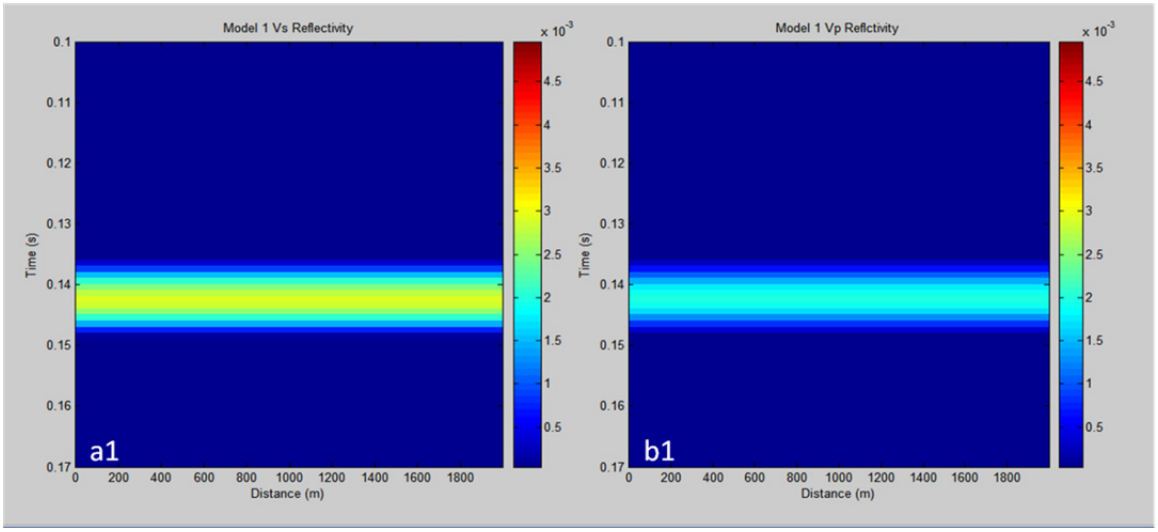

FIG. 7. Inversion results of the velocity reflectivity for the model 1 as conversional impedance contrast interface. a1 is a shear wave velocity reflectivity. b1 is a P wave velocity reflectivity.

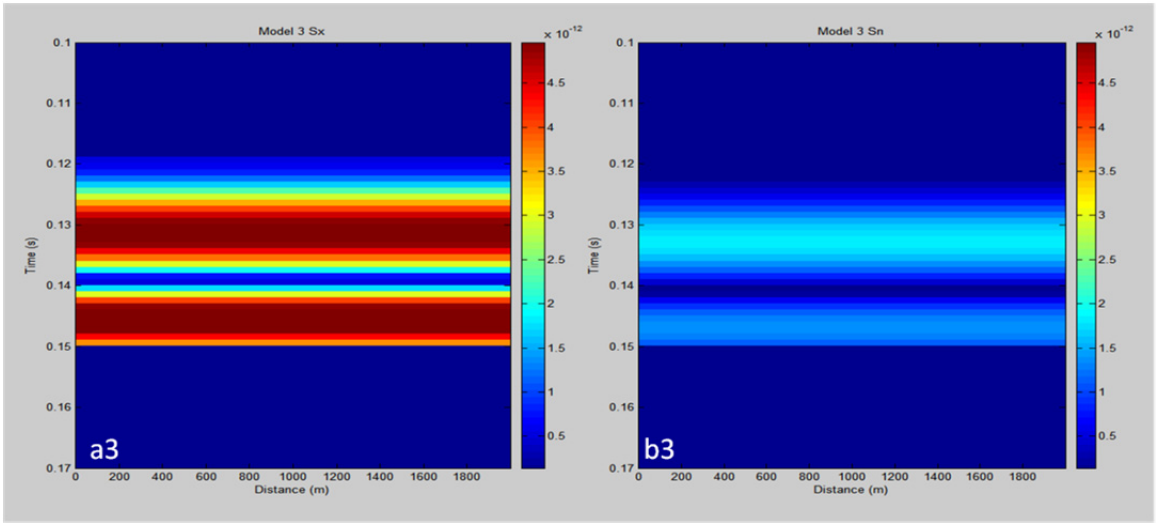

FIG. 9. Inversion results of the tangential and normal compliances of the model 3 as a fracture embedding in single medium. a3 is for a tangential compliance of the fracture. b3 is for a normal compliance of the fracture.

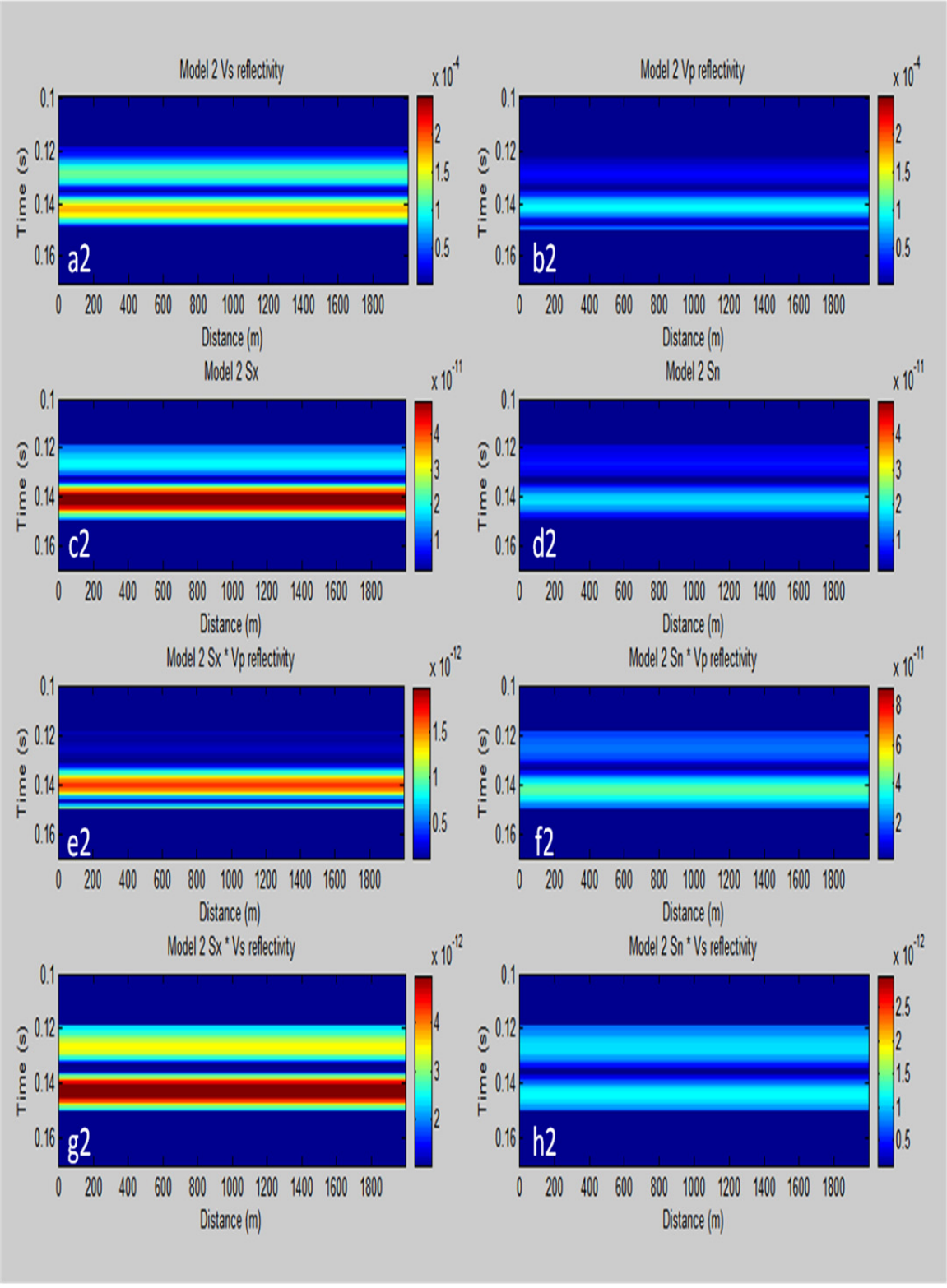

FIG. 8. Inversion results of the media elastic parameters for the model 2 as a fractured impedance contrast interface. There are: a2, b2 are for velocities reflectivity. c2, d2 are for fracture compliances. e2, f2 are the fracture compliances multiplying the P wave velocity reflectivity. g2, h2 are the fracture compliances multiplying the shear wave velocity reflectivity.

REFERENCES

Aki, K., and Richards, P. G., 1980, Quantitative seismology, theory and methods, volume 1: W H Freeman and Co, Cambridge Press, 144 – 154.

Backus, G. E., 1962, Long-wave anisotropy produced by horizontal layering: J. Geophys. Res., 66, 4,427-4,440, 1962.

Chaisri, Siriporn., 2002, A study of a nonwelded contact interface : exact and approximate formulas for P-SV reflection and transmission coefficients, and frequency domain raytracing, Ph.D. thesis, University of Calgary.

Crampin, S., 1985, Evidence for aligned cracks in the Earth's crust: First Break, 3, no. 3, 12-15.

Coates, R.T.; and Schoenberg, M., 1995, Finite-difference modeling of faults and fractures, Geophysics, 60, 1514-1526.

Cui, X.Q., Lines, L.R., 2011, PP, PS Reflection And Transmission Coefficients For a Non-welded Interface Contact With Anisotropic Media: SEG Annual Meeting, September 18 - 23, 2011.

Cui, X.Q., Lines, L.R., and Edward S. Krebes., 2013, Numerical Modeling for Different Types of Fractures: Geoconvention, 2013.

Downton, J. and B. Roure, 2010, Azimuthal simultaneous elastic inversion for fracture detection: SEG, Expanded Abstracts, 29, 263.

Gardner, G. H. F., Gardner, L.W. and Gregory, A. R., 1974, Formation velocity and density - The diagnostic basics for stratigraphic traps: Geophysics, 39, 770-780.

Gray, F.D. [2011] Methods and systems for estimating stress using seismic data. United States Patent Application,20110182144A1. http://www.google.com/patents/US20110182144.pdf?source=gbs_overview_r&cad=0.

Hood, J. A., and Schoenberg, M., 1989, Estimation of vertical fracturing from measured elastic moduli: Journal of Geophysical Research, 94, 15,611–15,618.

Hsu, C. J., and Schoenberg, M., 1993, Elastic waves through a simulated fractured medium: Geophysics, 58, 964–977.

Hudson,. A. 1981. Wave speeds and attenuation of elastic waves in material containing cracks. Geophysical Journal of the Royal Astronomical Society 64, 133-150.

Korn, M., and Stockl, H., 1982, Reflection and Transmission of Love Channel Wave at Coal Seam, Discontinuities Computed with a Finite Difference Method. Journal of Geophysics, 50: 171-176

Lines, L.R., Daley, P.F., and Embleton, J.E., 2008, The resolution and detection of "subseismic" high-permeability zones in petroleum reservoirs: The Leading Edge May 2008 vol. 27 no. 5 664-669

Lines, L. R., SlawinskI, R.,and bording, R. P. 1999. A recipe for stability of finite-difference wave-equation computation.Geophysics 64, 967–969.

Lines, L.R. and Treitel, S. 1984, *Tutorial: A Review of Least-Squares Inversion and its*. *Application to Geophysical Problems, Geophysical* Prospecting 32, 159-186, 1984.

Nichols, D.. Muir. F., and Schoenberg, M., 1989, Elastic properties of rocks with multiple sets of fractures: 59th Ann. Internat. Mtg., Soc. Expl. Geophys.. Expanded Abstracts, 471474.

Pyrak-Nolte, L.J., L.R, Myer., and N.G.W. Cook., 1990b, Transmission of seismic wave across single natural fracture: J. Geophys. Res. 95. 8617-8638.

Slawinski., Raphael A., and Edward S. Krebes., 2002, Finite-difference modeling of SH-wave propagation in nonwelded contact media: Geophysics. vol. 67, pp. 1656-1663, No5

Ruger, Andreas., 1998, Variation of P-wave reflectivity with offset and azimuth in anisotropic media: Geophysics 63, 935.

Schoenberg, M., 1980, Elastic wave behavior across linear slip interfaces, J. Acoust. Soc. Am., 68, 1516-1521.

Schoenberg, M., and Douma, J., 1988, Elastic wave propagation in media with parallel fractures and aligned cracks: Geophysical Prospecting, 36, 571-590.

Schoenberg, M., and Muir, F., 1989, A calculus for finely layered anisotropic media: Geophysics, 54, 581–589.

Schoenberg, M., and Sayers, C.M., 1995, Seismic anisotropy of fractured rock: Geophysics, 60, 204-211.

Smith, G.C., and Gidlow, P.M., 1987, Weighted stacking for rock property estimation and detection of gas: Geophys. Prosp., 35,993.1014

Thomsen Leon., 1986, Weak elastic anisotropy: Geophysics. vol. 51, 1954-1966

Yanghua, Wang., 1999, Approximations to the Zoeppritz equations and their use in AVO analysis, Geophysics, vol. 64, no. 6 (november-december 1999); P. 1920-1927,4 figs., 1 table.